RSC Advances

ROYAL SOCIETY OF CHEMISTRY

www.rsc.org/advances

Electrochemical modulation of plasma fibronectin surface conformation enables filament formation and control of endothelial cell-surface interactions

Mahdi Dargahi[1], Valentin Nelea[2], Aisha Mousa[2], Sasha Omanovic[1], and Mari T. Kaartinen[2,3*]

[1]Department of Chemical Engineering, McGill University, 3610 University Street, Montréal, Québec, Canada H3A 0C5

[2]Faculty of Dentistry, McGill University, Montreal, QC, Canada H3A 0C7

[3]Faculty of Medicine, Department of Medicine, Division of Experimental Medicine, McGill University, Montreal, QC, Canada, H3A 1A3

*Corresponding author

KEYWORDS: Plasma fibronectin, gold surface, electrochemistry, surface functionalization, endothelial cells, cell adhesion

Table of contents entry

Electrochemical modulation of a gold surface charge induces conformational changes in fibronectin when immobilized on the surface. A negatively-charged surface yields an open and filamentous fibronectin which significantly improves endothelial cell adhesion.

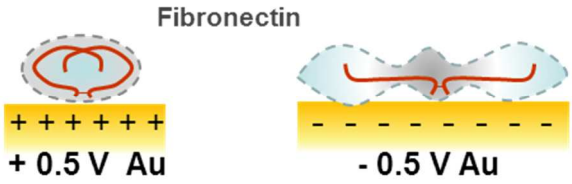

Abstract

Control of cell behavior to increase biocompatibility of implantable medical devices can be improved by protein coatings. Plasma fibronectin (FN) is a circulating soluble protein capable of assembling into insoluble filaments, fibrils and networks which promote various cellular processes and tissue integrity. FN fibrillogenesis is initiated by a conformational change, which has been proposed to involve charge-mediated opening of its structure. In this study, we have used a bare gold surface polarized electrochemically in the double-layer region to modulate its charge from highly positive to highly negative. The negatively charged surface promoted molecular extension and assembly of FN into beaded filaments and creation of a stable protein coating as examined by atomic force microscopy and electrochemical differential capacitance measurements. Gold surfaces with open and filamentous FN showed significantly improved endothelial cell adhesion while allowing formation of cell-cell contacts. Such surfaces may be used to promote rapid endothelialisation of cardiovascular stents.

Introduction

Protein adsorption onto a surface from tissue and body fluids such as plasma is a process that immediately occurs upon introduction of any artificial material (*e.g.* medical/dental implants) to the *in vivo* biological environment of the human body[1-4]. The resulting protein layer, and protein conformation on the surface, then defines the physical, biochemical, morphological and topographical cues presented by the surface[5, 6] and is thus involved in all subsequent interfacial biological interactions between the material and cells of the resident tissue.[7, 8] Accordingly, the nature of the proteins that adsorb from the fluids onto the implant surface is of great importance regarding cell-material interactions as they can result in either favourable or adverse cellular and tissue responses.[7, 9-12] An example of undesired protein adsorption is that of fibrinogen from plasma onto surfaces of coronary artery metallic stents which attracts platelets and can thus increase the risk of thrombosis, delay re-endothelialisation, and cause immune cell infiltration as well as smooth muscle cell proliferation,[13-15] leading to restenosis and implant failure. Also, the inflammatory reaction to a foreign object can cause fibrous encapsulation of implantable devices causing their failure.[16, 17] For successful integration of stents with endothelium and surrounding vascular tissue, it would be desirable that the stent surface be pre-coated with a protein that is capable of promoting rapid endothelial cell adhesion and abundant cell-cell interactions to create a native-like monolayer of epithelial cells that would block any further protein and other cell type interactions with the stent.

Fibronectin (FN) is a ubiquitous extracellular matrix glycoprotein required for the adhesion, survival, proliferation, and differentiation of adhesion-dependent cells.[18, 19] FN

is a dimeric protein consisting of two protein chains bound to one another by a disulfide bond. FN exists in two main soluble forms: as circulating plasma FN made by hepatocytes in liver, and as cellular FN synthesized by certain tissue-resident cells[20, 21]. Both forms arise from alternate splicing of one gene and support cell adhesion, regulate various cellular functions, and are capable of assembling into insoluble elongated extracellular matrix fibrils from their generally globular form. Generally, this macromolecular assembly − a fibrillogenesis process − requires FN binding to cellular integrins, along with cellular tension to stretch, unfold and open the FN molecule, which in turn leads to exposure of FN self-assembly sites.[22, 23] This initial FN assembly then leads to the formation of filaments and fibrils, which are subsequently converted to an insoluble extracellular matrix network to which cells bind to, migrate and proliferate on under *in vivo* circumstances.[22] Globular, soluble plasma FN molecule exists only in the circulation.

Immobilization of plasma FN onto materials is a commonly-used method to increase the biocompatibility of many different types of biomaterials.[24-27] Physical adsorption of FN on the biomaterial surface (the dip-coat method) is commonly used, but in this case the protein is only weakly attached. Although very simple, this surface-modification method for implantable materials is not efficient because the adsorbed FN layer can easily detach from the surface under the shear stresses of blood flow, exposing the bare surface to a wide range of plasma proteins such as fibrinogen, leading to adverse consequences such as restenosis or fibrosis, and ultimately implant failure. Therefore, in order to increase the long-term biocompatibility and stability of stents, it would be ideal to: (*i*) irreversibly immobilize FN on the stent surface, and (*ii*) achieve a favourable

surface conformation, protein density and/or fibrillar form of FN that would better mimic cell adhesion as it occurs *in vivo*, and (*iii*) have this surface promoting rapid endothelial cell adhesion.

Several groups, including ours, have shown experimentally that FN can adopt different conformations on surfaces of different topography and charge.[28-35] This has also been demonstrated by molecular modeling/computer simulation studies.[36, 37] Pernodet *et al*.[33] showed that negatively charged sulphonated polystyrene surfaces induced formation of FN molecular networks, and we demonstrated that a negative polysulphonate surface can open and elongate FN from its globular conformation and assemble it into filamentous structures with a degree of periodicity.[32] Also, recent work demonstrated that electrospun polymer fibers can induce the formation of FN networks.[34, 35] Since FN occurs naturally as a fibrillar network in tissues, it is possible that these macromolecular assemblies created on negatively charged surfaces may also behave differently regarding cell adhesion.

As referred to in the literature cited above, the surface charge of various materials was modulated by using different surface chemistries. However, this approach influences not only the substrate surface charge and its distribution, but also its surface chemistry, morphology, structure and other physico-chemical properties (chemical reactivity, and topography), thus making it difficult to study the sole influence of surface charge on protein-interfacial interactions. In order to examine the latter, we have employed an electrochemistry-based approach in which a gold electrode surface charge was controlled *in situ* by using a potentiostat and an electrochemical cell, without changing the other physico-chemical/structural properties of the surface. FN was adsorbed to the surfaces

and the subsequent FN/gold surface interactions were investigated. Gold was selected as a metal substrate for the following reasons*:* (*i*) its wide electrochemical double-layer region allows modulation of the substrate surface charge from being highly negative to being highly positive without initiating any faradaic reactions and changes in other physico-chemical, structural and topographical properties of the surface, and (*ii*) it is relatively inert towards other biological elements. In addition to investigating the influence of gold surface charge on the conformation of FN at this surface, we also aimed to examine the effect of electrochemically modified gold-FN surfaces on endothelial cell adhesion and the formation of a cellular monolayer. We report that electrochemically polarized *negative* gold surfaces promote FN opening and filament formation, and these surfaces are rapidly populated by endothelial cells that form both cell-matrix and cell-cell attachments.

Results

Electrochemical characterization of a gold electrode surface

Figure 1 [curve (*a*)] shows the linear polarization voltammetry profile of a gold electrode in 0.1 M phosphate buffer (PB) solution. A wide electrochemical double-layer region is noticed between –0.9 V and +0.7 V. The hydrogen evolution reaction (HER) occurs at potentials negative of –0.9 V while at potentials positive of +0.7 V the gold surface oxidizes to form an oxide layer. The oxygen evolution reaction (OER) follows, as observed at around +1.4 V. In order to avoid the interference of the faradaic reactions (HER, OER and gold oxidation) on FN adsorption, the adsorption of FN on the gold

electrode surface was done at constant potentials within the electrochemical double-layer region, *i.e*. at –0.5 V, open circuit potential (OCP, +0.1 V), and +0.5 V.

Since the main objective of the present work was to investigate the influence of surface charge on FN-gold surface interactions, we determined the potential range in which the gold surface is positively and negatively charged. Curve (*b*) in Figure 1 represents the differential capacitance (DC) response of the gold surface in the same 0.1 M phosphate buffer electrolyte solution. A minimum of capacitance is observed at around –0.1 V, indicating that the surface carries no net charge at this potential under the experimental conditions employed (potential of zero charge, PZC). At potentials below PZC, the gold surface becomes negatively charged, while at potentials above PZC the surface is positively charged. Thus, FN adsorption experiments were performed at –0.5 V Au, OCP Au, and +0.5 V Au. The interaction of FN with the gold surface was investigated under conditions in which the surface carries charges with values at the extremes of negative and positive (Figure 1).

Fibronectin adsorption onto polarized gold electrode surfaces

Polarization modulation infrared reflection adsorption spectroscopy (PM-IRRAS) measurements

PM-IRRAS was first used in this study to validate the existence of FN on gold. When studying surface-adsorbed proteins using PM-IRRAS, the spectral region of interest includes amide bands, which are characteristic of all proteins. In this study, the analysis was focused on the Amide I band because of its well-defined, strong signal. Figure 2 shows PM-IRRAS spectra of FN adsorbed on a gold surface polarized at three

different potentials (–0.5 V, OCP, and +0.5 V). Assuming that the overall dipole moment angle of adsorbed FN does not change significantly relative to the surface normal, the intensity increase of Amide I (Figure 2) indicates, in the first approximation, that the surface concentration of adsorbed protein increases with the increase of potential in the positive direction. To better visualize this trend, the area under each Amide I band *i.e.* its integrated intensity, $A_{Amide\ I}$ was determined and presented as an inset to Figure 2. X-ray photoelectron spectroscopy (XPS) results (data not shown) have also revealed that the nitrogen content on the sample prepared at +0.5 V is 91±21% higher than that on the sample prepared at –0.5 V; the control sample (the bare gold surfaces kept in the FN-free solution) did not yield any nitrogen peaks by XPS, confirming that the nitrogen content on the two FN-modified samples is solely attributable to the presence of protein on the surface. The FN molecule is overall negatively charged at the investigated solution pH (isoelectric point ≅ 5.0). Thus, it is to be expected that FN would interact more favourably with a more positively-charged gold surface, resulting in a higher FN surface concentration. In conclusion, Figure 2 indicates that electrostatic forces between FN molecules and the surface play a significant role in the adsorption of protein on the gold surface.

Adsorption kinetics

In order to obtain fundamental information on the initial stages of the FN-gold surface interactions, the kinetics of FN adsorption were investigated as a function of electrode potential using differential capacitance (DC). Figure 3a shows the dependence of relative DC of gold electrode on adsorption time at various electrode potentials.

Taking into account that the relative DC is proportional to the protein surface concentration, the plot demonstrates that at a constant FN bulk concentration, the surface coverage of adsorbed FN increases rapidly immediately upon initiation of the protein adsorption process, and then gradually levels off into a plateau for the two positively-charged surfaces (+0.5 V and OCP: +0.1 V). However, Figure 3a shows that the FN adsorption kinetics at the negatively charge surface (–0.5 V) are different. During the first 6 minutes of adsorption, the relative DC follows the same trend at all three potentials. However, on the gold substrate surface polarized at –0.5 V, the relative DC reaches a maximum value after *ca.* 10 minutes of adsorption, followed by a gradual decrease to a constant value, attained after *ca.* 80 minutes of adsorption, indicating the attainment of adsorption equilibrium. This drop indicates that either desorption of FN occurs after 10 minutes of initial adsorption, or some structural changes in the adsorbed protein conformation on the gold surface commence after 10 minutes of adsorption. It will be explained shortly below (Figure 4) that the latter assumption is the most probable cause of the relative DC decrease. The difference in the relative DC values observed at 80 minutes at the three potentials in Figure 3a is in agreement with the results in Figure 2; with an increase in substrate surface potential, both the relative DC (Figure 3a) and integrated intensity (Figure 2) increase, indicating an increase in surface concentration of FN.

The next step was to evaluate the stability of the FN layer formed on the gold surface. In these experiments, the gold surface was prepared in the same way as in the adsorption experiments discussed previously. The background PM-IRRAS spectrum was recorded using a clean gold surface, followed by the adsorption of FN on the surface

from a 0.001 g/L FN solution in PB at +0.5 V or −0.5 V for 3 hours. Then, a PM-IRRAS spectrum was recorded to determine the amount of FN adsorbed onto the gold substrate. This was followed by immersing the surface in a FN-free PB solution under OCP conditions (an implant in the human body is at OCP). The amount of FN on the surface was then monitored at specific time intervals. Figure 3b shows the variation of FN surface concentration with time over a period of 21 days, presented in terms of normalized integrated intensity (with respect to the initially-adsorbed FN). FN adsorbed on the negatively-charged surface (–0.5 V) remained fully adsorbed on the surface even after 21 days, while the sample functionalized by FN under the positive polarization conditions (+0.5 V) experienced a *ca*. 12% decrease in the surface amount of FN. The results in Figure 3b thus demonstrate that FN is most likely covalently attached to the gold surface and is thus very stable, especially the FN layer adsorbed under negative polarization. Indeed, our XPS data of the surfaces indicate that the actual bonding between FN and gold occurred *via* S-Au bonds, suggesting the involvement of free cysteine thiol-groups of FN in this stable interaction. Figure 4 shows a XPS spectrum of the gold surface modified by FN at −0.5 V, displaying a peak centered in the 159-165 eV region. As reported in the literature, the thiol-gold bond yields a 2p response doublet structure centered at around 162-163 eV.[38] The same values are also reported for sulphur-metal bonds on stainless steel[39], iron[40], nickel[41] and silver[42]. The spectrum in Figure 4 displays a doublet peak at 161.7 eV and 163.2 eV, thus confirming the presence of FN on the surface and the formation of a sulphur-gold bond.

Atomic force microscopy (AFM) measurements

We next examined the effect of gold electrode surface charge on the conformation of adsorbed FN protein molecules. AFM imaging was performed on FN-adsorbed gold electrode surfaces kept at potentials of −0.5 V, OCP, and +0.5 V. Figure 5 shows the conformation of individual FN molecules as adsorbed onto positively-charged gold surfaces (+0.5 V Au). FN possesses here a compact, closed conformation with molecules showing a globular shape (Figure 5a). Analysis of the average sizes of these FN structures from the height profiles of the compacted structures (Figure 5b) shows that the protein has an obloid shape, being 45 nm in width and 4.5 nm in height, as schematically represented in Figure 5c.

Analysis of FN conformation on a negatively-charged surface (−0.5 V Au) reveals two populations of FN molecules − elongated FN and filamentous FN (Figure 6 and Figure 7, respectively). The extended, open FN conformation included FN molecules that have an open structure with most of the molecules having a multi-nodal structure with the widths of the nodules ranging from 7 nm to 22 nm (Figure 6a). The length of FN molecules measured 142 nm on average, while the heights were approximately half the size (2-3 nm in range) of those of the FN closed-conformation obloids (Figure 6b,c). The molecular dimensions of FN measured here at positive and negative potentials are typical for FN molecules in closed, and respectively, open conformations, as reported in the literature [30, 32, 43]. Examination of multiple scans performed in various areas on negatively-charged (−0.5 V Au) samples found that, in addition to the FN open conformation, large numbers of these molecules assembled unidirectionally to form long filaments, with lengths from hundreds of nm up to several micrometers and apparent widths in the range of 8-34 nm (Figure 7a,b). Filaments showed a characteristic bead-on-

a-string structure with connected beads of diameters in the range of 10-22 nm. The density of the beads was variable, being lower (Figure 7a, yellow arrow) or higher (Figure 7a, red arrow) on various filament segments. Beads showed a certain periodicity of their arrangement along the filament (Figure 7b). An average inter-bead distance of *ca*. 92 nm was measured for less-dense beaded structures, while this distance shortened to 40-45 nm on filament portions having a higher density of beads (Figure 7c). Filament heights were in the range of 2.7-4.5 nm, with the largest values residing at the level of the beads, suggesting that the filaments are firmly settled onto the substrate surface. Furthermore, these measured heights demonstrate that the beads are not deriving from chains of closed FN, which have larger heights (4-5 nm). Heights and widths of most filaments were close to those observed for elongated FN molecules (Figure 6), indicating that filament assembly proceeded by longitudinal alignment and association of molecules in open conformation in a similar head-to-tail fashion with overlaps of connected molecular domains forming the beads (Figure 7c). Filaments also appeared to have the capability of joining other filaments by lateral attachment (Figure 7a, orange arrow), and thicker filaments (25-34 nm in width) should be the product of such events of lateral attachment/fusion of thin filaments. Systematic investigation of positively charged gold samples (+0.5 V) revealed no filament formation. At OCP (+0.1 V, which is also a positively charged surface), a population of compact FN spheroids was observed with no filaments or any other feature that would suggest incipient stages FN alignment (data not shown).

Cell-surface interactions

We next examined the cell adhesion properties of the FN-gold surfaces. Figure 8 shows the surface density of HUVEC endothelial cells after 4 hours of attachment to the three different FN-modified surfaces (black bars) as well as to their corresponding bare gold controls (Ctrl, gray bars) as analyzed by crystal violet staining and quantification. All of the FN-containing surfaces (black bars) yielded a significantly higher cell density than the surfaces with no FN (gray bars) (Figure 8). The highest cell surface density was obtained on the gold surface coated by FN at –0.5 V. The cell density represented an approximately 60% increase in comparison to the bare (control) surface polarized at the same potential. This surface also supported approximately 40% more cells than the Au surface modified by FN at +0.5 V. On the other hand, no difference in cell surface density was noted on the three control surfaces (gray bars). Consequently, the results in Figure 8 provide evidence that (*i*) the presence of FN on the gold surface promotes cell adhesion, (*ii*) the surface charge-induced changes in conformation of adsorbed FN (Figures 6 and 7) greatly influence subsequent cell/surface interactions, and (*iii*) that once FN is adsorbed onto the gold surface and adopts its conformation, it most likely remains in such a conformation during the interaction of cells with the surface.

Analysis of the cell layers by scanning electron microscopy (SEM) (Figure 9) showed that the endothelial cell density was visibly higher on the Au surface onto which FN was adsorbed at –0.5 V than on the other two surfaces (+0.5 V and OCP), as evidenced by the darkness in the field of view generated by tightly packed cell crowding (quasi-forming a monolayer). The data is in agreement with the quantitative results presented in Figure 8. Although all FN-containing surfaces supported cell adhesion, the

cells adherent to the FN/OCP Au and FN/+0.5V Au appeared larger, indicative of increased spreading on the surface (a cell is outlined by the dashed red line, Figure 9). Increased spreading, in turn, suggests that cells strongly react to the surface. Considering that the endothelial cells primarily should adhere to each other *via* VE-cadherin-mediated cell-cell adhesions to form a monolayer, tight attachment to the surface is not desirable. To examine the cell-cell adhesions on these surfaces, we visualized VE-cadherin by immunofluorescence microscopy. Figure 10a shows the cell-cell interaction sites (actin, green) and VE-cadherin (red) of the endothelial cells attached to the gold surface modified by FN at the three different potentials. The surface on which FN was adsorbed at –0.5 V showed stronger VE-cadherin staining compared to cells on the FN/OCP and FN/+0.5V surfaces, which show very poor VE-cadherin on the cell periphery, even when the cells are at the same distance one from each other as on the FN/–0.5V surface. This indicates that cells on the two positively-charged surfaces (OCP and +0.5 V) may be reacting with the surface rather than forming a monolayer with each other. Total levels of VE-cadherin in these cells were not different, as seen by Western blot analysis (Figure 10b) confirming that only its localization was changed upon attachment. Further Western blot analyses showed that endothelial cells on all surfaces had very similar phosphorylation of focal adhesion kinase (FAK), which is a signaling molecule that becomes activated upon attachment to a surface *via* focal adhesions. This indicates that only the FN/–0.5V surface allowed both cell-surface and cell-cell adhesions to occur simultaneously. The increased cell spreading on the FN/OCP and FN/+0.5V surfaces was not mediated *via* increased cellular FN (EDA-FN) production. All surfaces promoted EDA-FN synthesis at a similar level, as seen in Figure 10b. Collectively, these

observations suggest that only the FN conformation on the surface is the main factor mediating the observed cell behavior.

Figure 10c illustrates the proposed interpretation of the morphology of endothelial cells attached to gold surfaces. Figure 10c-(*i*) shows endothelial cell attachment to globular FN on the +0.5 V Au − the cell is spread and flattened, and VE-cadherin is mostly intracellular. FAK phosphorylation (pFAK), indicative of adhesion to the surface, is occurring simultaneously. Figure 10c-(*ii*) shows endothelial cell behavior after attachment to the extended/filamentous FN on the −0.5 V Au surface − cell-cell adhesions are established *via* VE-cadherin, while the cells simultaneously also adhere to the surface (pFAK).

Discussion

Induction of rapid endothelialisation of coronary artery stents is of great importance for their successful integration. Failure to attract endothelial cells to populate stent surfaces can lead to fibrin and platelet adhesion which can induce thrombosis.[44, 45] Delayed endothelialisation can also lead to increased smooth muscle cell proliferation and restenosis, and complete stent failure. [44] Surface coating of the stents plays a critical role in guiding subsequent cellular events that occur in relation to the stent in the *in vivo* environment. FN is a major cell adhesion protein, abundantly present in plasma (about 300 μg/mL in humans) and thus it is expected to adsorb onto medical devices from tissue fluids. FN conformation and assembly into supramolecular assemblies defines its functionality in tissues. FN conformation and folding is modulated by hydrophobicity, pH, ionic strength of its fluid environment as well as fibrillogenesis and electrostatic

changes that occur to its binding partners (protein/polymer or surface).[29-35] The aim of our work here was to examine the behaviour of FN adsorbed on chemically inert gold surfaces that were simply modified electrochemically to carry different charge (either positive or negative), and to subsequently examine the interaction of endothelial cells with these surfaces. We report here that FN molecules adsorbed onto negatively-charged gold surfaces assume extended, open and filamentous conformations which allow better endothelial cell binding as well as establishment of monolayer organisation with cell-cell interactions. Thus, we conclude that the success of coronary artery stents may potentially be improved by modifying their surfaces with a FN coating where the FN molecules are in an extended, open and filamentous conformation, which can be achieved prior to the stent implantation by the electrochemical method described herein.

FN adsorption onto surfaces is a common method to increase adhesion of many cell types onto cell culture plastic or other types of surfaces that require better biocompatibility. Our work suggests that endothelial cells may adopt more native state-like behavior − including epithelial monolayer formation − on open, extended and filamentous FN. While endothelial cells also adhered to surfaces where FN was in its compact from, this induced cell spreading and not cell-cell adhesion. This indicates that the cell adhesive properties of closed/compact FN versus open/filamentous FN are different. While the mechanism behind the altered behavior of different FN surfaces remains unknown, it is possible that for endothelial cells the open/filamentous FN provides a sufficiently 'light' adhesion environment. Furthermore, it is also possible that during FN extension and self-assembly, the availability of the cell-adhesion sites and associated synergistic sites is altered. Such self-assembly and fibrillogenesis also changes

the coverage on the surface which very likely also contribute to cell behavior. Also, other researchers have reported similar endothelial cell behavior towards FN; Vallieres *et al.*[46] reported that FN-functionalized-fused silica can promote endothelial cell adhesion with the preferred morphology when FN was immobilized in an open conformation. Conversely, Wan *et al.*[47] recently reported that unfolding of FN decreases its ability to support adipocyte cell adhesion. These observations suggest that controlling protein conformation may allow fine tuning of biocompatibility. Future studies will be directed towards examining this and how different cell types behave on these charged FN-gold surfaces.

Many reports have addressed conformational changes in FN on surfaces having various degrees of water wettability, *i.e*. hydrophilicity vs. hydrophobicity.[30, 48, 49] FN was found in a compact, closed conformation when FN was adsorbed on hydrophobic surfaces, in contrast to studies using hydrophilic surfaces where FN was dominantly found in an open, elongated state. Taken together, those results indicated that the hydrophilic substrates have a net negative charge on their surface, and the authors suggested that the negative charge induces the opening of FN. This hypothesis has been confirmed in studies of negatively charged functionalized polyelectrolyte substrates[32, 33] and by our present study. Using silica (SiO_2) substrates (hydrophilic), Bergkvist *et al.*[30] suggested that the negative charge on the silica surface interferes with the electrostatic intramolecular interactions of FN, thus destabilizing the forces (hydrophobic in nature) that keep FN in its compact form. Conversely, on methylated silica substrates (hydrophobic, and no charge at the surface), there is no destabilization of intramolecular FN interactions that keep FN in its compact conformation, and FN was found to keep its

compact conformation upon surface adsorption. Keselowsky *et al*.[48] reported increased cell adhesion on FN-adsorbed substrates functionalized with self-assembling monolayers (SAMs) with hydroxyl- and carboxyl-terminations in comparison to methyl-terminated SAMs, suggesting that the presentation of the integrin-binding domain of FN is altered by the surface chemical moieties. Charge on a substrate surface has a higher influence on FN elongation (opening) than the surface wettability (hydrophilicity) itself since more elongated FN forms on surfaces of a similar wettability (silica *vs.* mica), but having different charge surface density[30]. Also, enhancement of FN fibril formation with the increase of the negative charge density of a sulphonated surface was reported[33]. This charge should be negative to allow FN to open, because the positive charge on surfaces with comparable wettability to silica − like our aminopropyltriethoxysilane, poly-L-lysine and poly-allylamine surfaces previously studied[32] − do not induce FN elongation. Moreover, sulphonated polyelectrolytes are less hydrophilic than aminopropyltriethoxysilane, poly-L-lysine and poly-allylamine[32], but, since surface charge competes against and prevails over wettability, elongated FN forms.

FN filament and fibril assembly *in vivo* is a cell-mediated process, although it is not yet fully established how FN molecules organize themselves into filaments and fibers. Thus, experimentally creating native state-like FN fibrils and networks/matrices without cells is challenging. FN assembly in a staggered manner has been proposed theoretically,[50] and growing evidence suggests that the electrochemical environment drives both opening and assembly of FN. The prevailing idea is that FN is maintained in its closed/compact conformation by the interaction of modules $III_{2\text{-}3}$ (negative) and $III_{12\text{-}14}$ (positive)[51]. It was proposed by Pernodet *et al.*[33], that the negatively-charged surface

draws the molecule open *via* interacting with III_{12-14} modules. In our previous report[32], we also showed FN opening as well as the formation of periodic, beaded FN filaments on chemically-modified, negatively-charged polysulphonated surfaces, and in this present report we provide further evidence that, indeed, both events can occur on a negatively-charged surface in the absence of charge-controlling / functionalizing chemical groups (functional organic monolayers, coatings, *etc.*). The filaments likely form as a consequence of opening and extending the FN structure that allows inter-molecular interactions of self-assembly sites. As previously proposed by us [32], beading may form *via* overlap of larger modules III_{1-7}. While the ability to create *in vitro* exact replicas of *in vivo*-occurring FN fibrils remains to be achieved, this new information may provide cues on how to begin the engineering of such native structures to elicit desired cellular responses.

Our results also demonstrate that FN is tightly attached to the negatively-charged gold surface and is thus forming a very stable coating. The higher stability of the FN layer adsorbed on a negative surface may be explained by the open surface conformation and the filamentous FN having multiple interaction sites with the gold. Kowalczynska *et al.* [52] investigated the interaction of FN with bare and sulphonated polystyrene surfaces and reported tighter bonds between FN and substrate and increased adhesion of lymphoid leukemia L1210 cells when FN molecules were adsorbed onto the sulphonated surface in an extended conformation. Better attachment of NIH 3T3 fibroblasts[53] and bovine aortic endothelial cells[54] was found on FN-adsorbed hydrophilic glass where FN has a more open conformation than on FN-adsorbed a hydrophobic surface. Here we show that the electrochemically-assisted adsorption of FN onto a gold surface is not only efficient in

controlling the conformation of FN, but that it also yields an irreversibly-adsorbed FN layer on negatively-polarized gold surfaces. Our XPS results suggest that the FN molecule chemically interacts with the gold surface by creating an S-Au bond, with the sulphur atom most likely originated from the cysteine residues of FN. The exact thiol-residues in FN molecule involved in the interaction remains unknown.

The control of FN conformation *via* charge, its stability on the surfaces, as well as allowing for subsequent cell interactions opens a range of possibilities in the area of development of medical implants. For example, a commercial metal stent surface could be electrochemically functionalized by using a patient's own FN (previously extracted from blood collection samples) immediately prior to the stent implantation, thus potentially increasing the stent's biocompatibility and endothelialisation potential while decreasing the possibility of in-stent restenosis.

Conclusion

Endothelial cell interactions with a metal surface can be increased by electrochemically providing a negative charge to the metal and then adsorbing FN onto this surface. The negatively-charged gold surface promotes the extension and opening of the FN protein resulting in the formation of FN filaments that are tightly and stably bound to the gold surface. The open and filamentous FN surface promotes endothelial cell adhesion while allowing epithelial monolayer formation and the establishment of appropriate cell-cell interactions. Positively-charged gold surfaces do not have these same properties for adsorbed FN − while they allowed endothelial cell adhesion and promoted cell spreading, they did not facilitate cell-cell adhesions. This work suggests

new possibilities for improving currently-used bare metal cardiovascular stents by relatively simple charge-mediated FN adsorption to promote rapid endothelialisation and subsequent tissue integration.

Experimental

Substrates

Glass slides (1.5 cm × 1.5 cm area; EMF Corp., Ithaca, NY, USA) coated with a 100 nm-thick gold layer sputtered onto 5 nm-thick chromium tie-layer were used as substrates for FN adsorption. The gold slides were first cleaned in an ultrasonic bath in acetone for 30 min, then rinsed with deionized water (Nanopure, resistivity 18.2 MΩ cm), ethanol, and acetone, and dried with pure argon (99.998%). Prior to each protein adsorption experiment, gold samples were electrochemically cleaned/pre-treated in 0.5 M sulphuric acid (Fisher Scientific, Montreal, QC, Canada) by cyclic polarization (50 cyclic sweeps between +1.5 V and –0.3 V vs. Ag/AgCl at a scan rate of 200 mVs^{-1}). This treatment ensures that the substrates are of the same surface topography and physicochemical properties. For the AFM imaging, fresh-cleaved muscovite mica substrates (1 cm × 1 cm area; Electron Microscopy Sciences, Washington, PA, USA) coated with 40 nm-thick gold layer sputtered onto 5 nm-thick chromium tie-layer (Nanotools Microlab, McGill University) were used. The root mean square roughness of gold-coated glass and mica surfaces was 1.2 ±0.1 nm and 0.8 ±0.1 nm, respectively, as measured by AFM of areas of 1 μm × 1 μm.

Protein solutions

Bovine plasma fibronectin (Sigma-Aldrich, St. Louis, MO, USA) was used as received. Fibronectin was at 1 g / L in a solution of Tris Buffered Saline (TBS), 50 mM Tris, 150 mM NaCl, pH 7.4. The working protein solutions were prepared by diluting FN in 0.1 M phosphate-buffer (PB) (monobasic potassium phosphate, KH_2PO_4, Sigma-Aldrich, St. Louis, MO, USA) pH 7.4 at concentrations in the range of 0.001-0.01 g/L.

Electrochemical cell and electrodes

The electrochemical experiments were performed in a 10 mL glass cell. The electrolyte was 0.1 M PB solution in which FN was dissolved. The counter electrode was a platinum mesh, while the reference electrode was an Ag/AgCl electrode (Innovative Instruments Inc., Indian Trail, NY, USA). Two working electrodes were used: one was a platinum wire, while the other was the gold slide onto which FN was adsorbing. The purpose of the platinum electrode was to ensure that the gold slide was always polarized at the specified potential while being withdrawn from the electrolyte for further analysis. This was necessary in order to prevent surface potential from drifting to open-circuit during the removal from the electrolyte. Wherever stated in the manuscript, potentials are expressed with respect to the Ag/AgCl reference electrode.

Differential capacitance

An *in situ* differential capacitance (DC) electrochemical technique was used to investigate the interaction of FN with a gold surface polarized at a constant potential within the electrochemical double-layer region, during the protein adsorption period. An

Autolab potentiostat/galvanostat/frequency response analyzer (PGSTAT30/FRA2, Ecochemie, Utrecht, Netherlands) controlled through GPES/FRA v 4.9.5 software was used.

Polarization modulation infrared reflection adsorption spectroscopy

PM-IRRAS was applied to confirm *ex situ* the presence of adsorbed FN and to measure the surface concentration of FN adsorbed onto the gold substrates. A Fourier transform infrared (FTIR) spectrophotometer (Tensor 27) equipped with an external PM50 polarization module and a liquid nitrogen-cooled MCT detector (Bruker Optics Inc., Billerica, MA, USA) was used. The wavenumber of the polarization modulator was fixed at 1600 cm^{-1}. All samples were scanned for 300 times with a 3 cm^{-1} resolution and an aperture setting of 5 mm. The incident beam angle with respect to the surface normal was set to 85 degrees for all experiments.

X-ray photoelectron spectroscopy

XPS measurements were performed using a ThermoFisher Scientific K-Alpha Spectrometer equipped with an argon ion gun. The X-ray polychromatic source was AlKα (1486.6 eV). A survey spectrum was first recorded to identify all elements present on the sample surface, followed by recording high-resolution spectra. An energy step size of 0.1 eV was used for high-resolution elemental analysis.

Atomic force microscopy

AFM imaging of FN molecules adsorbed on differently polarized gold surfaces was performed using a multi-mode scanning probe microscope (Digital Instruments Nano-Scope IIIa, MultiMode, SPM, Santa Barbara, CA, USA) operating in tapping mode in air at ambient temperature. AFM probes were PointProbePlus (NANOSENSORS™ STM, Neuchatel, Switzerland) with 10-130 Nm^{-1} force constant and a typical radius of curvature of the tip at its apex less than 7 nm. All AFM scans presented here and those that have been used for the analyses were performed at 0.5-1 Hz scan rates on specimen areas of 5 μm × 5 μm or smaller. The amplitude setpoint was set as high as possible allowing scans with minimized forces applied to the sample. Ranges of feedback control parameters were in the ranges as follows: integral gain 1–2, proportional gain 2–4, look-ahead gain, 0–0.8. Post-processing of AFM images was performed using WSxM 5.0 Develop 1.1 software[55]. Post-processing of images presented here included planeing, flattening and adjustments of brightness, contrast, Z-axis scale and Z-axis scale offset, as well as the use of a palette color setting (Flame.lut) that allows distinction of fine height variations of surface features at the sub-nanometre level. Z-axis profiles traced unidirectionally over the specimen surface were recorded using the profiling function of the WSxM software.

Scanning electron microscopy

SEM was used to image the surface of the gold substrate after cell attachment. The substrates were gently washed with PBS and fixed with 2.5% (v/v) glutaraldehyde (Fisher). The fixed samples were subsequently dehydrated with a graded series of 10

minutes of ethanol immersions (30 to 100 v/v %) and a graded series of amyl acetate in ethanol solutions (25 to 100 v/v %). The substrates were further dried using a critical point dryer for 2 hours. Samples were examined with an S-4700 field-emission gun microscope (Hitachi High Technologies, Pleasanton, CA, USA) and images were recorded using Quartz PCI v. 6.0 software.

Cell adhesion assay

To evaluate the response of cells to FN-modified gold surfaces, human umbilical vein endothelial cells (HUVECs) were used. HUVECs were a generous gift from Dr. Elaine Davis (McGill University). Cells were cultured in a humidified 37°C incubator at 5% CO_2 in endothelial growth medium (EGM-2 BulletKit, Cedarlane/Lonza, ON, Canada). Cells were plated onto bare or FN-modified gold surfaces that were placed inside non-treated 12-well culture plates (BD, New Jersey, USA). Plating density was 50,000 cells per cm^2 (Wisent, St-Jean-Baptiste, QC, Canada) and cells were allowed to interact with the surfaces for 4 hours. At the incubation endpoint, the EGM-2 medium was removed and the cells were washed twice with phosphate-buffered saline (PBS). The cells were then fixed with 1% glutaraldehyde in PBS for 10 minutes at room temperature. After fixation, cells were washed two times with PBS and then stained with 0.5% crystal violet in 20% methanol in PBS with continuous gentle shaking of the plates for 20 minutes at room temperature. The solution was removed and the wells were washed twice with distilled water and dried in ambient air. The cell-bound stain was dissolved by incubating the wells with 1% sodium dodecyl sulfate (SDS) overnight in the dark. The optical density was measured spectrophotometrically at 595 nm using a microplate reader.

Immunofluorescence microscopy

Cells were plated on gold surfaces at a density of 50,000 cells per cm^2 and allowed to adhere for 4 hours in a humidified 37°C incubator at 5% CO_2. Cells were then rinsed with PBS, and fixed using sterile 3.7% formaldehyde in PBS for 10 minutes at room temperature. Gold surfaces were blocked for 30 minutes in 2% bovine serum albumin (BSA) in PBS with gentle shaking at room temperature. Cells were incubated with rabbit VE-Cadherin antibody (Cell Signaling Technology, Danvers, MA, USA) overnight at 4°C diluted in 0.1% BSA in PBS, and then incubated for one hour with Alexa Fluor 568 secondary rabbit antibody (orange). Gold surfaces were washed at least three times with 0.1% BSA. Actin cytoskeleton was visualized by Alexa Fluor 594 Phalloidin (green) and nuclei were visualized with DAPI (blue) (Invitrogen, Burlington, ON, Canada). Gold surfaces were mounted using Prolong Gold™ anti-fade mounting medium (Invitrogen). Immunofluorescence images were taken using Zeiss digital camera mounted on a Zeiss fluorescence microscope (USA).

Protein extraction and Western blotting

Protein was extracted from HUVEC cells after 4 hours of plating cells on the gold surfaces using protein lysis buffer (RIPA buffer). Protein concentrations were determined using bichinonic acid (BCA) protein assay (Fisher Scientific, Nepean, Canada). Twenty (20) μg protein from each sample was dissolved in SDS-loading buffer containing β-mercaptoethanol and boiled for 5 minutes at 100°C, followed by electrophoretic separation of proteins on 10% SDS-polyacrylamide gels and subsequently transferred onto polyvinylidene difluoride membrane (PVDF) (Bio-Rad, Mississauga, Canada).

Membranes were blocked for one hour in 5% non-fat dry milk in Tris Buffered Saline-Tween 20 (TBS-T), and then incubated with primary antibodies diluted in TBS-T at 4°C against the following antigens: Focal Adhesion Kinase (FAK), phospho-FAK (Tyr397), VE-cadherin (rabbit polyclonal antibodies, Cell Signaling Technology) followed by one hour incubation with rabbit secondary antibody conjugated with horseradish peroxidase (Cell Signaling Technology). β-actin antibody (rabbit polyclonal antibody, Sigma) was used as a protein loading control. Bands were visualized using the spray-on ECL Western blotting substrate reagent (ZmTech Scientific, Montreal, QC, Canada) and chemiluminescence was detected using Hyperfilm ECL (GE Healthcare, Baie d'Urfé, QC, Canada).

Acknowledgements

This study was supported by grants to MTK from the Canadian Institutes of Health Research (CIHR) and to SO from Natural Sciences and Engineering Research Council of Canada (NSERC) and the Fonds de recherche du Québec – Nature et technologies (FRQNT).

Notes and references

1. T. A. Horbett, *Cardiovasc Pathol*, 1993, **2**, S137-S148.
2. M. Wahlgren and T. Arnebrant, *Trends in Biotechnology*, 1991, **9**, 201-208.
3. M. C. L. Martins, D. Wang, J. Ji, L. Feng and M. A. Barbosa, *Biomaterials*, 2003, **24**, 2067-2076.
4. Z. S. Xiang, M. , in *Encyclopedia of Medical Devices and Instrumentation*, John Wiley & Sons, Inc., New York, 2nd edn., 2006.
5. J. M. Anderson, A. Rodriguez and D. T. Chang, *Seminars in Immunology*, 2008, **20**, 86-100.
6. P. Asuri, S. S. Bale, S. S. Karajanagi and R. S. Kane, *Current Opinion in Biotechnology*, 2006, **17**, 562-568.
7. C. J. Wilson, R. E. Clegg, D. I. Leavesley and M. J. Pearcy, *Tissue Engineering*, 2005, **11 (1-2)**, 1-18.
8. L. Bacakova, E. Filova, M. Parizek, T. Ruml and V. Svorcik, *Biotechnology Advances*, 2011, **29**, 739-767.
9. P. J. Molino, M. J. Higgins, P. C. Innis, R. M. I. Kapsa and G. G. Wallace, *Langmuir*, 2012, **28**, 8433-8445.
10. A. Dolatshahi-Pirouz, T. Jensen, M. Foss, J. Chevallier and F. Besenbacher, *Langmuir*, 2009, **25 (5)**, 2971-2978.
11. A. Dolatshahi-Pirouz, T. Jensen, D. C. Kraft, M. Foss, P. Kingshott, J. L. Hansen, A. N. Larsen, J. Chevallier and F. Besenbacher, *Acs Nano*, 2010, **4 (5)**, 2874-2882.
12. A. G. Hemmersam, K. Rechendorff, M. Foss, D. S. Sutherland and F. Besenbacher, *J Colloid Interf Sci*, 2008, **320 (1)**, 110-116.
13. A. L. Bailly, A. Laurent, H. Lu, I. Elalami, P. Jacob, O. Mundler, J. J. Merland, A. Lautier, J. Soria and C. Soria, *J Biomed Mater Res*, 1996, **30**, 101-108.
14. J. A. Chinn, T. A. Horbett and B. D. Ratner, *Thromb Haemostasis*, 1991, **65**, 608-617.
15. L. K. Lambrecht, B. R. Young, R. E. Stafford, K. Park, R. M. Albrecht, D. F. Mosher and S. L. Cooper, *Thrombosis research*, 1986, **41 (1)**, 99-117.
16. J. M. Anderson, *Ann Rev Mater Res*, 2001, **31**, 81-110.
17. B. G. Keselowsky, A. W. Bridges, K. L. Burns, C. C. Tate, J. E. Babensee, M. C. LaPlaca and A. J. Garcia, *Biomaterials*, 2007, **28**, 3626-3631.
18. P. Elter, R. Lange and U. Beck, *Colloids and Surfaces B: Biointerfaces*, 2012, **89**, 139-146.
19. J.-H. Seo, K. Sakai and N. Yui, *Acta Biomaterialia*, 2013, **9**, 5493-5501.
20. R. Pankov and K. M. Yamada, *J Cell Sci*, 2002, **115**, 3861-3863.
21. E. L. George, E. N. Georgeslabouesse, R. S. Patelking, H. Rayburn and R. O. Hynes, *Development*, 1993, **119**, 1079-1091.
22. P. Singh, C. Carraher and J. E. Schwarzbauer, *Annu Rev Cell Dev Bi*, 2010, **26**, 397-419.
23. W. S. To and K. S. Midwood, *Fibrogenesis Tissue Repair*, 2011, **4**.
24. G. Li, P. Yang, X. Guo, N. Huang and R. Shen, *Cytokine*, 2011, **56**, 208-217.

25. R. Müller, J. Abke, E. Schnell, F. Macionczyk, U. Gbureck, R. Mehrl, Z. Ruszczak, R. Kujat, C. Englert, M. Nerlich and P. Angele, *Biomaterials*, 2005, **26**, 6962-6972.
26. K. W.-C. Sungtae, M.;Jung-Seok, L.; Jae-Kook, C.; Ui-Won, J.; Hyeong-Cheol, Y.; In-Seop, L.; Seong-Ho, C. , *J Periodontal Implant Sci*, 2011, **41**, 242-247.
27. A. J. Garcia and C. D. Reyes, *J Dent Res*, 2005, **84**, 407-413.
28. J. Ballester-Beltrán, P. Rico, D. Moratal, W. Song, J. F. Mano and M. Salmerón-Sánchez, *Soft Matter*, 2011, **7**, 10803-10811.
29. L. Donlon, D. Nordin and D. Frankel, *Soft Matter*, 2012, **8**, 9933-9940.
30. M. Bergkvist, J. Carlsson and S. Oscarsson, *Journal of Biomedical Materials Research Part A*, 2003, **64A**, 349-356.
31. H. M. Kowalczyńska, R. Kołos, M. Nowak-Wyrzykowska, J. Dobkowski, D. Elbaum, A. Szczepankiewicz and J. Kamiński, *Journal of Biomedical Materials Research - Part A*, 2009, **91**, 1239-1251.
32. V. Nelea and M. T. Kaartinen, *Journal of Structural Biology*, 2010, **170 (1)**, 50-59.
33. N. Pernodet, M. Rafailovich, J. Sokolov, D. Xu, N. L. Yang and K. McLeod, *Journal of Biomedical Materials Research - Part A*, 2003, **64 (4)**, 684-692.
34. M. Salmeron-Sanchez, P. Rico, D. Moratal, T. T. Lee, J. E. Schwarzbauer and A. J. Garcia, *Biomaterials*, 2011, **32**, 2099-2105.
35. J. Ballester-Beltrán, M. Cantini, M. Lebourg, P. Rico, D. Moratal, A. J. García and M. Salmerón-Sánchez, *Journal of Materials Science: Materials in Medicine*, 2012, **23**, 195-204.
36. J. J. Gray, *Curr Opin Struc Biol*, 2004, **14**, 110-115.
37. C. Y. Liao, Y. Xie and J. Zhou, *Rsc Adv*, 2014, **4**, 15759-15769.
38. T. M. Willey, A. L. Vance, T. van Buuren, C. Bostedt, L. J. Terminello and C. S. Fadley, *Surf Sci*, 2005, **576**, 188-196.
39. H. Dadafarin, E. Konkov, S. Omanovic and *Int. J. Electrochem. Sci*, 2013, **8**, 369 - 389.
40. G. Kataby, T. Prozorov, Y. Koltypin, H. Cohen, C. N. Sukenik, A. Ulman and A. Gedanken, *Langmuir*, 1997, **13**, 6151-6158.
41. Z. Mekhalif, F. Laffineur, N. Couturier and J. Delhalle, *Langmuir*, 2003, **19**, 637-645.
42. Y. H. Wang, Q. Yu, Y. Zhang, Z. R. Guo, N. Gu and K. D. Wesche, *Appl Surf Sci*, 2004, **229**, 377-386.
43. D. L. Hasty, H. S. Courtney, W. A. Simpson, J. A. Mcdonald and E. H. Beachey, *J Cell Sci*, 1986, **81**, 125-141.
44. A. Farb, A. P. Burke, F. D. Kolodgie and R. Virmani, *Circulation*, 2003, **108**, 1701-1706.
45. A. Undas, J. Zalewski, M. Krochin, Z. Siudak, M. Sadowski, J. Pregowski, D. Dudek, M. Janion, A. Witkowski and K. Zmudka, *Arterioscl Throm Vas*, 2010, **30**, 276-U287.
46. K. Vallières, P. Chevallier, C. Sarra-Bournet, S. Turgeon and G. Laroche, *Langmuir*, 2007, **23**, 9745-9751.

47. A. M. D. Wan, E. M. Chandler, M. Madhavan, D. W. Infanger, C. K. Ober, D. Gourdon, G. G. Malliaras and C. Fischbach, *Biochimica et Biophysica Acta (BBA) - General Subjects*, 2013, **1830**, 4314-4320.
48. B. G. Keselowsky, D. M. Collard and A. J. García, *Journal of Biomedical Materials Research - Part A*, 2003, **66**, 247-259.
49. H. M. Kowalczynska, R. Kolos, M. Nowak-Wyrzykowska, J. Dobkowski, D. Elbaum, A. Szczepankiewicz and J. Kaminski, *Journal of Biomedical Materials Research - Part A*, 2009, **91 (4)**, 1239-1251.
50. D. M. P. Peters, Mosher, D.F., ed. P. D. Yurchenco, Birk, D.E., Mecham, R.P, Academic Press, San Diego, CA, 1989, pp. 315–350.
51. K. J. Johnson, H. Sage, G. Briscoe and H. P. Erickson, *J Biol Chem*, 1999, **274**, 15473-15479.
52. H. M. Kowalczyńska, R. Kołos, M. Nowak-Wyrzykowska, J. Dobkowski, D. Elbaum, A. Szczepankiewicz and J. Kamiński, *Journal of Biomedical Materials Research Part A*, 2009, **91A**, 1239-1251.
53. L. Baugh and V. Vogel, *Journal of Biomedical Materials Research Part A*, 2004, **69A**, 525-534.
54. D. J. Iuliano, S. S. Saavedra and G. A. Truskey, *J Biomed Mater Res*, 1993, **27**, 1103-1113.
55. I. Horcas, R. Fernandez, J. M. Gomez-Rodriguez, J. Colchero, J. Gomez-Herrero and A. M. Baro, *Rev Sci Instrum*, 2007, **78**, 013705.

Figure legends

Figure 1. (a) Linear polarization voltammogram of a gold electrode recorded in 0.1 M phosphate buffer at a scan rate of 200 mV s^{-1}. (b) Differential capacitance voltammogram of a gold electrode recorded in 0.1 M phosphate buffer at a scan rate of 2.5 mV s^{-1}, frequency of 25 Hz; *ac* amplitude of ±5 mV. PZC = potential of zero charge; OCP = open circuit potential.

Figure 2. PM-IRRAS spectra of FN adsorbed onto a gold surface substrate recorded after 3 hours of immersion of the substrate in a solution of 0.010 g L^{-1} FN in 0.1 M phosphate buffer at (1) –0.5 V, (2) OCP, and (3) +0.5 V. Inset shows the dependence of the integrated intensity of the Amide I band of FN on the potential applied to the gold substrate. Symbols are mean values of at least four measurements and error bars represent their corresponding standard deviation. With an increase in gold surface potential, the amount of adsorbed FN also increases.

Figure 3: (a) The kinetics of FN adsorption on the gold surfaces presented in terms of the dependence of gold electrode relative differential capacitance on adsorption time. FN was adsorbed from a solution of 0.001 g L^{-1} in 0.1 M phosphate buffer with substrates kept at (1) –0.5 V, (2) OCP, and (3) +0.5 V. The behaviour of –0.5 V indicates possible surface conformational changes of FN occur with time during its adsorption. (b) Dependence of normalized integrated intensity of FN Amide I band on the desorption time. The FN layer was pre-adsorbed on the gold surface polarized at (○) –0.5 V and (Δ) +0.5 V. Such FN-

modified samples were immersed for a total of 21 days in a FN-free solution of 0.1 M phosphate buffer and PM-IRRAS measurements were performed at the indicated times. Symbols are mean values of at least four measurements and error bars represent their corresponding standard deviation. The surface concentration of FN on the negatively-charged gold surface remains constant, indicating that FN is irreversibly adsorbed on the surface.

Figure 4. XPS high-resolution sulphur spectrum (dot line) of FN adsorbed on a gold surface substrate recorded after 3 hours of immersion of the substrate in a solution of 0.010 g L^{-1} FN in 0.1 M phosphate buffer at –0.5 V. The sulphur peak was deconvoluted into two peaks with maxima at 161.7 eV and 163.2 eV (dashed lines), and the resulting sum spectrum is represented with solid line.

Figure 5. AFM analysis of a FN conformation on a positively-charged (+0.5 V) FN-gold surface. (a) AFM height images showing a closed conformation of the FN molecules. Color pictures in the second row are post-processed images rendering height details. (b) Representative height profile of a FN molecule showing a globular, obloid shape. (c) Schematic model of a closed FN molecule with corresponding measured sizes.

Figure 6. AFM analysis of an extended FN conformation on a negatively-charged (–0.5 V) FN-gold surface. (a) AFM height images showing an extended, open FN conformation that is seen on as three smaller globular units of the protein. Color pictures in the second row are post-processed images rendering details in height. (b) Representative height

profile of a FN molecule showing an elongated shape (c). Schematic model of an elongated FN molecule with corresponding measured sizes.

Figure 7. AFM analysis of the formation of filamentous FN self-assembled structures on a negatively-charged (–0.5 V) FN-gold surface. (a) AFM height images showing FN filaments with a beads-on-a-string structural appearance. Filaments have lengths of a few micrometres with visible beading (less dense, yellow arrow or more dense, red arrow) suggesting that FN is capable of lateral attachment on this surface (orange arrow). (b) AFM height post-processed image showing a portion of a FN self-assembled filament and its corresponding height profile where the periodic, ordered, beaded arrangement is revealed. Beads occur every 90/95 nm or 40/45 nm along the filament. (c) Schematic model of how FN molecules may arrange into filaments *via* partial overlap that creates the periodic beaded structure.

Figure 8. Quantification of HUVEC cell adhesion, after 4 hours of cell-surface interaction time, to bare, non-modified gold surfaces (Ctrl, gray), and to FN-gold surfaces onto which FN was pre-adsorbed at different surface potentials (black). All surfaces containing FN supported cell adhesion significantly better than without FN. The negative surface (–0.5 V) with FN supported significantly more cells than the positive (+0.5 V) and OCP surfaces with FN. Values represent the mean of three replicates. Error bars are the standard deviations. (*) $p < 1\times10^{-3}$; (**) $p < 1\times10^{-4}$.

Figure 9. Scanning electron microscopy analysis of HUVEC cells on bare, non-modified gold surfaces (Ctrl) and gold surfaces modified with a FN layer adsorbed on the negative (–0.5 V), OCP and positive (+0.5 V) gold surface of different charge. The control (Ctrl) surfaces only poorly supported cell adhesion. All the FN-modified surfaces supported cell adhesion. Cell density was visibly higher on the negative surface with FN. The red dashed line outlines the cell shape emphasizing that HUVECs on the OCP and +0.5 V surfaces with FN are more extensively spread and appear larger. Cells on the negative surface with FN (–0.5 V) are attached to each other forming a very dense monolayer, and appear smaller in size.

Figure 10. Analysis of cell-cell and cell-substrate adhesion molecules by immunofluorescence microscopy and Western blotting. (a) Immunofluorescence microscopy analysis of VE-Cadherin localization on HUVECs plated on FN-gold surfaces with different charge. The negative surface (–0.5 V) clearly shows VE-Cadherin (red) at cell-cell adhesion sites indicative of cell-cell attachment. The FN/OCP and FN/+0.5V gold surface show significantly less of this staining despite the close proximity of cell to one another indicating that proper cell-cell attachment did not occur. (b) Western blot analysis of focal adhesion kinase phosphorylation (pFAK, Tyr397) shows that all surfaces support cell-substrate adhesion in a similar manner. Cellular FN (EDA-FN) and VE-Cadherin are synthesized by the HUVECs on all surfaces. Actin was used as a loading control. (c) Proposed HUVEC behavior on the positive and negative gold surfaces. The positive surface that supports the globular FN conformation, promotes cell spreading (pFAK active), but not cell-cell adhesion. VE-cadherin is found in the

intracellular space. The negative surface that promotes filamentous FN conformation, allows both cell-cell (VE-cadherin found at cell-cell attachment sites) and cell-substrate adhesion (pFAK active) to occur.

Figure 1

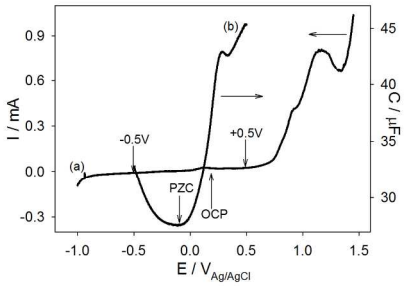

254x338mm (300 x 300 DPI)

Figure 2

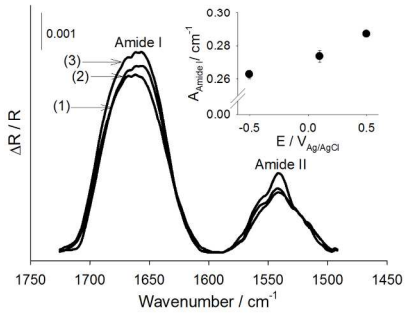

254x338mm (300 x 300 DPI)

Figure 3

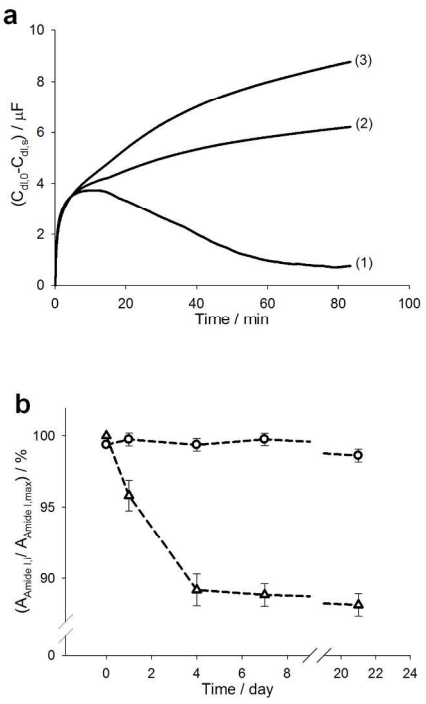

254x338mm (300 x 300 DPI)

Figure 4

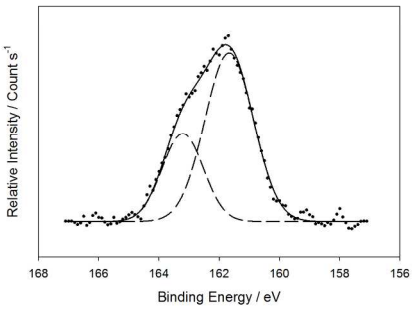

254x338mm (300 x 300 DPI)

Figure 5

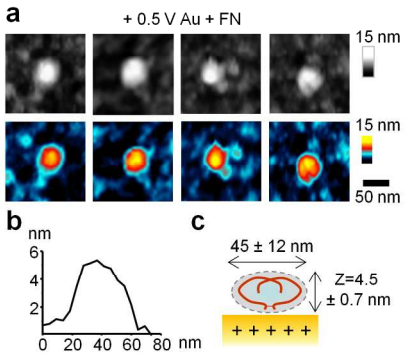

254x338mm (300 x 300 DPI)

Figure 6

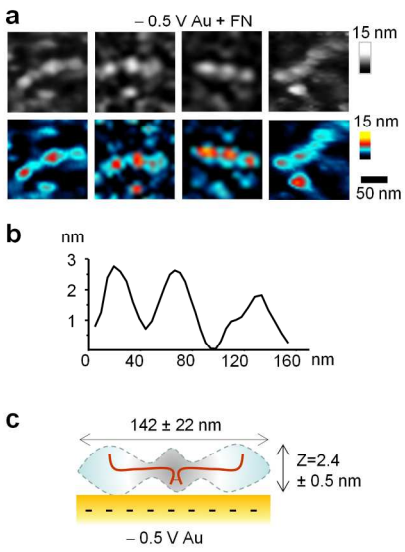

254x338mm (300 x 300 DPI)

Figure 7

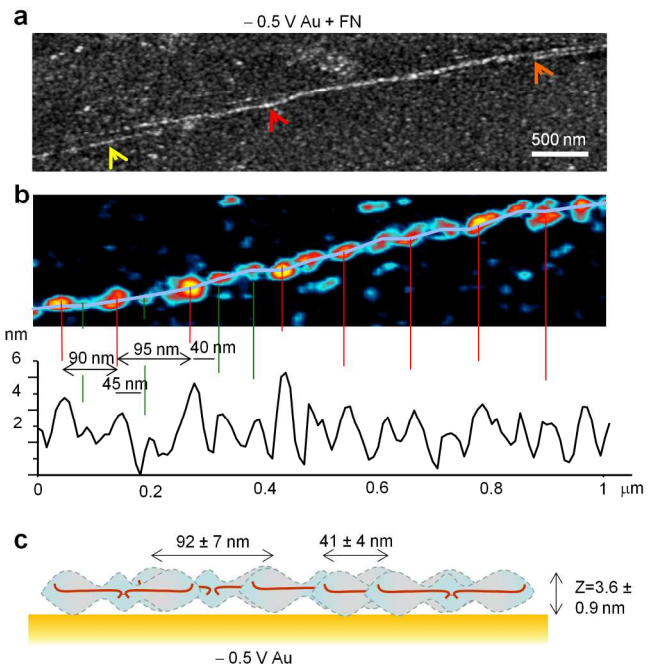

254x338mm (300 x 300 DPI)

Figure 8

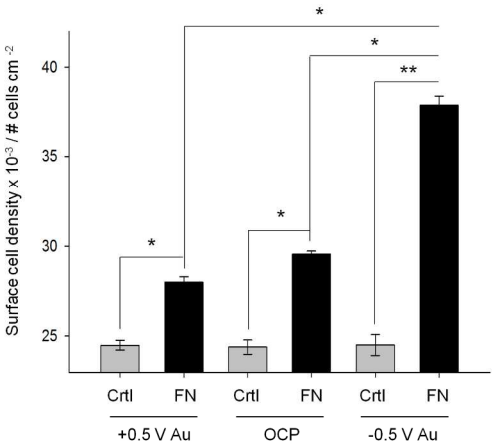

254x338mm (300 x 300 DPI)

Figure 9

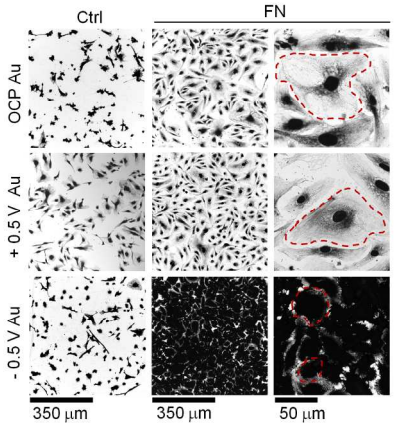

254x338mm (300 x 300 DPI)

Figure 10

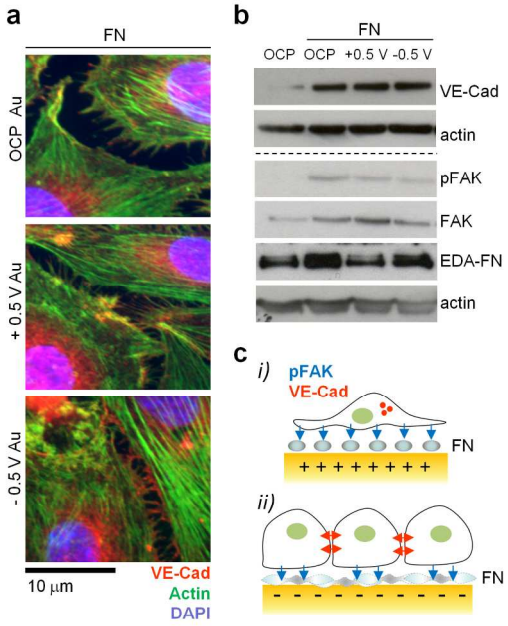

254x338mm (300 x 300 DPI)